



Long-Axis Spinning of an Optically Levitated Particle: A Levitated Spinning Top

Journal Article

Author(s):

Zielińska, Joanna A.; van der Laan, Fons; Normann, Andreas; [Reimann, Rene](#) ; Frimmer, Martin; [Novotny, Lukas](#) 

Publication date:

2024-06-21

Permanent link:

<https://doi.org/10.3929/ethz-b-000679766>

Rights / license:

[In Copyright - Non-Commercial Use Permitted](#)

Originally published in:

Physical Review Letters 132(25), <https://doi.org/10.1103/physrevlett.132.253601>

Funding acknowledgement:

863132 - Inertial Sensing Based on Quantum- Enhanced Levitation Systems (EC)
ETH-47 20-2 - Levitated Quantum Rotors (ETHZ)

Long-axis spinning of an optically levitated particle: A levitated spinning top

J. A. Zielińska,¹ F. van der Laan,^{1,2} A. Norrman,^{1,3} R. Reimann,^{1,4} M. Frimmer,¹ and L. Novotny^{1,*}

¹Photonics Laboratory, ETH Zürich, CH-8093 Zürich, Switzerland

²Center for Nanophotonics, AMOLF, 1098 XG Amsterdam, The Netherlands

³Center for Photonics Sciences, University of Eastern Finland, P.O. Box 111, FI-80101 Joensuu, Finland

⁴Quantum Research Center, Technology Innovation Institute, Abu Dhabi, UAE

(Dated: April 30, 2024)

An elongated object can be rotated around one of its short axes, like a propeller, or around its long axis, like a spinning top. Using optically levitated nanoparticles, short-axis rotation and libration have been systematically investigated in several recent studies. Notably, short-axis rotational degrees of freedom have been cooled to millikelvin temperatures and driven into GHz rotational speeds. However, controlled long-axis spinning has so far remained an unrealized goal. Here, we demonstrate controlled long-axis spinning of an optically levitated nanodumbbell with spinning rates exceeding 1 GHz. We show that the damping rate in high vacuum can be as low as a few millihertz. The high quality factor of 10^{12} and the exceptional stability of long-axis spinning open up applications in inertial torque sensing and studies of rotational quantum interference.

Introduction.— Cylindrically symmetric nanorotors, when trapped within linearly polarized optical tweezers, align their most polarizable (long) axis to the polarization direction of the tweezers. This results in libration of the rotor, i.e. torsional oscillations around an equilibrium angle driven by a linear restoring torque. In particular, two degenerate libration modes emerge, corresponding to oscillatory rotations around the two least-polarizable (short) axes. Significant advances have been made in controlling short axis rotations, with nanorotors being driven to spin at GHz rates [1–4], libration oscillations cooled down to mK temperatures [5–8], and several demonstrations of torque sensing [3, 9–12]. However, in all these studies the rotation around the long axis remained unconstrained and was driven by thermal fluctuations [5, 6, 13]. Introducing controlled long-axis spinning would complement the existing research on short axis rotations by enabling the simultaneous control of the rotational rate and the orientation of the rotation axis. This achievement would close a notable gap in the field and provide a valuable resource for inertial torque sensing.

A levitated gyroscope with competitive performance requires large angular momentum and low friction, which poses constraints on vacuum pressure and rotor size [14, 15]. Inertial torque sensing of rotations has been successfully demonstrated using levitated birefringent vaterite particles [14, 16, 17], but the relatively high absorption rate of these particles prevents optical trapping in ultrahigh vacuum (UHV). On the other hand, silica nanoparticles can withstand UHV conditions [18] and they can be fused together to generate particles with shape anisotropy, such as cylindrically symmetric dumbbells. Furthermore, silica nanorotors can be precisely controlled down to their fundamental quantum and thermodynamic limits [4, 6] and driven to rotate at GHz rates around their short axes [1–4]. Nonetheless, gyroscope applications rely on accurately monitoring the orientation

of the spinning axis of the rotor. This is not feasible for short-axis rotations, since the spinning axis aligns with the tweezer propagation direction and is not reliably detected [19]. Therefore, controlled spinning around the long axis is a key requirement for the realization of an optically levitated gyroscope, because it simultaneously enables fast spinning and accurate measurement of the spinning axis orientation.

Long-axis spinning is also an important resource for studying quantum interference in the orientational dynamics of nanorotors [20]. The angular momentum of a free quantum rotor is quantized and in principle it can be prepared in a single eigenstate [21]. Thanks to the cylindrical symmetry of the dumbbell, the spinning around the long axis is decoupled from other rotations and defines a *free rotational* degree of freedom with quantized angular momentum [21]. This is different from translational and librational modes, which are governed by harmonic dynamics or short-axis rotations that are coupled to each other. Thus, long-axis spinning is a prerequisite for the exploration of quantum rotational

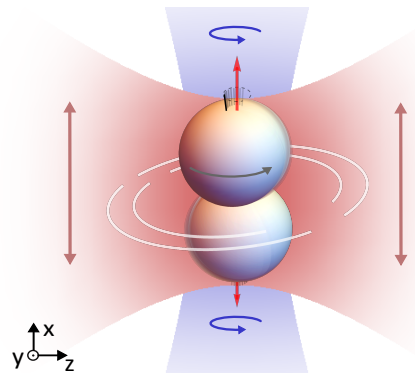


Figure 1. A nanodumbbell (not to scale) is trapped by an x polarized laser beam (red) and spun around its long axis by a circularly polarized spinning beam (blue).

effects [20], such as rotational revivals [22].

System under study.— Our system, illustrated in Fig. 1, consists of an optically levitated nanodumbbell exposed to a light field in a three-dimensional (3D) polarization state [23, 24]. The light field is composed of two parts: a strong tweezers field, linearly polarized along the x axis and propagating in the z direction, and a weak spinning beam, circularly polarized in the yz plane and propagating along the x direction. The tweezers field exerts a conservative restoring torque on the dumbbell, which aligns its long axis in the x direction and creates two libration modes around this equilibrium. In contrast, the circularly polarized beam generates a constant (and therefore non-conservative) torque, which drives the dumbbell into a spinning motion around its long axis. This torque arises from the optical spin [25, 26] carried by the beam together with absorption or imperfect cylindrical symmetry of the dumbbell [27–29].

The rotational dynamics of the nanodumbbell is thus governed by two libration angles φ and ϑ with respect to the x axis and the rotation angle ψ around its long axis [30]. In the presence of friction and assuming small-angle libration, the dumbbell’s spinning rate will accelerate until it reaches its steady-state value $\dot{\psi}_0 = \tau/(I_3\gamma_3)$ [1, 2, 4], where τ is the magnitude of the non-conservative torque, I_3 is the moment of inertia along the long axis, and γ_3 is the friction coefficient. The spinning motion reveals itself as a coupling $g = (I_3/2I_1)\dot{\psi}_0$ between the otherwise independent and harmonic libration modes, where I_1 is the moment of inertia along one short axis. The coupling leads to hybrid modes with eigenfrequencies

$$\Omega_{1/2} = \sqrt{\Omega_0^2 + g^2} \pm g, \quad (1)$$

where Ω_0 is the natural libration frequency [13, 30]. The higher frequency Ω_1 corresponds to nutation of the long axis, whereas the lower frequency Ω_2 is associated with precession of the long axis around the x direction [11, 13, 31, 32].

Most importantly, since the spinning rate is directly related to the torque and friction, with the torque scaling linearly with the spinning beam power [30], in our experimental implementation we can control the spinning rate via the optical power of the circularly polarized spinning beam and the chamber pressure. For high enough spinning rates, we can push our system far into the strong coupling regime, i.e., $g \gg \Omega_0$. In this regime we can approximate the eigenfrequencies as

$$\Omega_1 = 2g, \quad (2a)$$

$$\Omega_2 = \frac{\Omega_0^2}{2g}. \quad (2b)$$

As we increase the spinning rate of the dumbbell, the amplitude of nutation relative to precession decreases,

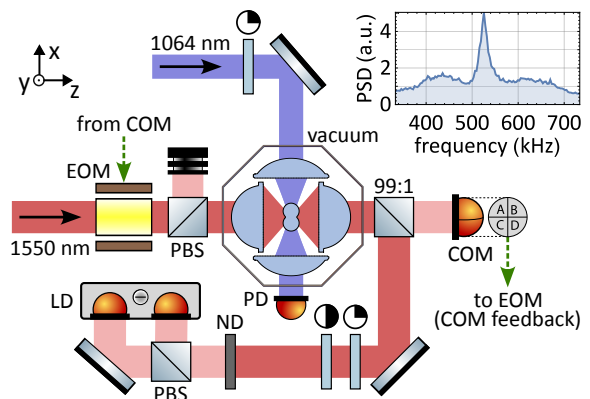


Figure 2. Experimental apparatus for spinning a dumbbell. The x polarized optical tweezers (wavelength 1550 nm) trap a dumbbell inside a vacuum chamber, while a circularly polarized beam (wavelength 1064 nm) propagating along x spins the dumbbell. Forward scattered light from the tweezers is split and subsequently sent to a quadrant photodiode and a balanced detector for center-of-mass (COM) and libration detection (LD), respectively. The detected COM motion is used to drive an electro-optic modulator (EOM) for feedback cooling x and y COM motion. The power of the spinning beam is monitored on a photodiode (PD). Inset: power spectral density (PSD, plotted in arbitrary units) of the libration motion of a trapped dumbbell recorded at a pressure of 0.1 mbar and without the spinning beam.

and the motion becomes dominated by slow precession with frequency Ω_2 [33].

Experimental setup.— In our experiment, depicted schematically in Fig. 2, dumbbells composed of two spherical silica nanoparticles (nominal diameter 143 nm) are optically trapped inside a vacuum chamber. The particles are loaded into the trap using a nebulizer. The tweezers beam forming the trap (wavelength 1550 nm, power 700 mW) is focused with an $\text{NA} = 0.8$ lens. The light scattered by the particle is subsequently collected by an $\text{NA} = 0.7$ lens and analyzed to detect librations in the xy plane and the center-of-mass (COM) motion along three main axes. For detecting the COM motion we use a quadrant photodiode, while libration is recorded with the help of a balanced detector as in [6]. In order to stabilize the position of the dumbbell inside the trap, we cool the x and y COM motion by parametric feedback [34] at pressures below 10^{-4} mbar.

We identify a trapped particle as a dumbbell when its COM x -to- y gas damping ratio is in the 1.1 – 1.15 range [2]. Another characteristic of dumbbells is their libration spectrum, which consists of a sharp libration peak at 525(3) kHz flanked by broad shoulders [5, 6, 13, 35], as shown by the inset of Fig. 2.

The spinning beam (wavelength 1064 nm, tunable power up to 120 mW) is focused onto the dumbbell by an $\text{NA} = 0.3$ lens with 7.5 mm focal length. The beam is

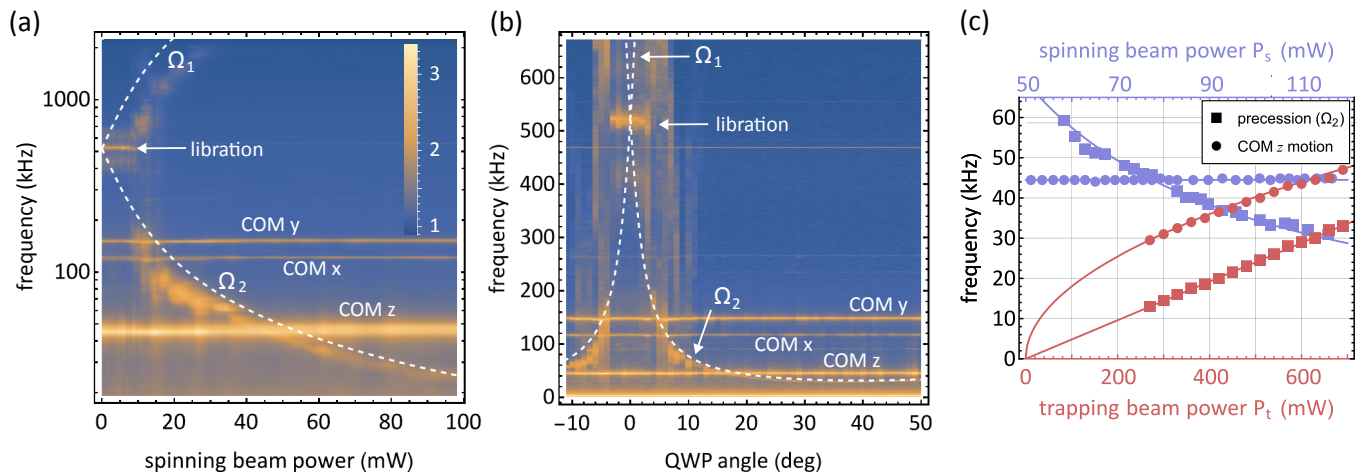


Figure 3. Power spectral density (PSD) of the detector signal as a function of (a) spinning beam power and (b) spinning beam polarization. The color scale for (a) and (b) depicts $\log(\text{PSD})$ in arbitrary units and the fits to Eq. (1) are shown as white dashed lines. Measurements (a)-(c) were performed at a pressure of 10^{-3} mbar. (a) As the spinning beam power is increased the libration peak splits into a high frequency nutation mode (Ω_1) and a low frequency precession mode (Ω_2). (b) As the quarter-wave plate (QWP) angle is rotated from 0° to 45° , the spinning beam polarization changes from linear to circular and the libration mode evolves into a precession mode with frequency Ω_2 . The spinning beam power is 100 mW. Note that the frequency scale is logarithmic in (a) whereas it is linear in (b). (c) Precession frequency Ω_2 and COM z-motion frequency as a function of trapping beam power (lower curves, spinning beam power 100 mW) and as a function of spinning beam power (upper curves, trapping beam power 700 mW). The spinning beam is circularly polarized. Fits according to Eq. (2b) are shown as solid lines.

then collected by another $\text{NA} = 0.3$ lens and its power is monitored using a photodiode. The polarization state of the spinning beam is controlled by a quarter-wave plate (QWP). Due to its low power and weak focusing, the spinning beam does not significantly alter the libration potential [30].

Results. — Figure 3(a) shows the measured libration spectra for different optical powers of the circularly polarized spinning beam at 10^{-3} mbar. For powers below 10 mW the thermally-driven spinning dominates, as evidenced by the constant libration frequency accompanied by the shoulder-like lineshape on both sides (cf. inset in Fig. 2). As we increase the spinning beam power above the 10 mW threshold, the libration mode splits into two hybrid modes created by the spinning motion. The white dashed curves are theoretical fits according to Eq. (1) which qualitatively agree with the experimental observations. We observe a broad high frequency nutation peak (Ω_1) and a narrow low frequency precession mode (Ω_2). As expected, the frequency Ω_1 of the nutation mode increases and its amplitude decreases [33] with increasing spinning beam power. The observed behaviour of Ω_2 frequency and Eq. (1) agree well for spinning beam powers above 40 mW, where the spinning rate of the dumbbell transitions into the fast spinning regime characterized by $g \gg \Omega_0$ [see also Fig. 3(c)]. Below 40 mW our model does not accurately predict the frequencies, including the 10 mW spinning beam power threshold for mode splitting

(also reported in Ref. [35]). We believe these deviations are related to the factors not included in our model, such as coupling to the COM motion, or imperfect shape of the dumbbell.

The torque τ experienced by the dumbbell can also be controlled by the polarization of the spinning beam. In Fig. 3(b) we show the measured libration spectra as a function of the QWP angle that changes the polarization of the spinning beam from linear to circular (see Fig. 2). When the QWP is set at 0° , the beam is linearly polarized in the z direction and has no detectable effect on the libration dynamics due to lack of optical spin. The coupling is dominated by thermally driven spinning, as if the spinning beam was absent. However, when the polarization becomes elliptical (QWP is rotated by approx. 5 degrees in either direction) the dynamics transitions abruptly into consistent spinning, as evidenced by the emerging low frequency precession mode (Ω_2). For circular polarization, Ω_2 decreases to approximately 30 kHz. The minimum of the precession frequency occurs around 35° due to birefringence of the vacuum viewport (included in the fit).

Next, we investigate the dependence of the precession frequency Ω_2 on the trapping beam power P_t and the spinning beam power P_s in the fast spinning regime ($g \gg \Omega_0$). The natural libration frequency Ω_0 was shown to depend on the square root of P_t [13]. This implies, according to Eq. (2b), that the precession frequency Ω_2 depends linearly on P_t , as long as the coupling rate

g is not affected by the trapping beam. The expected behavior is indeed confirmed by our measurements shown in Fig. 3(c). On the other hand, since the torque τ exerted on the dumbbell depends linearly on the spinning power P_s we expect, according to Eq. (2b), that Ω_2 scales inversely with P_s . We compare the behaviour of Ω_2 with that of the eigenfrequency of the COM z mode (which is expected to follow a square-root behavior on P_t and remain unaffected by changes in the spinning beam power P_s). The measured Ω_2 and COM z frequencies shown in Fig. 3(c) agree well with their respective predicted behaviors. We therefore conclude that Eq. (2b) correctly predicts the precession frequency in the fast spinning regime where $g \gg \Omega_0$. Note that the coupling strength surpasses the natural libration frequency even for moderate P_s , akin to deep ultrastrong coupling. According to Eq. (2b), the precession frequency of 30 kHz [see Figs. 3(a-c)] corresponds to a coupling rate $g = 2\pi \times 4.6$ MHz. Assuming our dumbbells have a length-to-diameter ratio of 1.8 (as in Ref. [27]), we estimate $I_3/I_1 \approx 0.6$, which yields a spinning rate of $\dot{\psi}_0 \approx 2\pi \times 15$ MHz.

Ringdown measurements.— The steady-state spinning rate $\dot{\psi}_0 = \tau/(I_3\gamma_3)$ is inversely proportional to the damping rate γ_3 , which in turn is proportional to the gas pressure. Thus, controlling the pressure allows us to tune $\dot{\psi}_0$ over several orders of magnitude. As described before, we can infer the dumbbell's spinning rate from the measured hybrid mode frequencies. However, in practice we are only able to detect the precession mode Ω_2 for spinning rates up to $\dot{\psi}_0 \approx 30$ MHz. The reason for this is two-fold: first, as $\Omega_2/(2\pi)$ decreases below 3 kHz it becomes obscured by electronic noise in our detection system [visible in Figs. 3(b) and 4(a)]; second, large spinning rates lead to large angular momenta which stabilize the system and reduce the precession amplitude which results in poor signal-to-noise in our measurements. We circumvent this problem by performing ringdown measurements, in which P_s is set to zero and the slowing down of the dumbbell's spinning rate is monitored [1]. For sufficiently high spinning rates thermal fluctuations can be ignored and the ringdown turns into a deterministic trajectory described by $\dot{\psi}(t) = \dot{\psi}(0)e^{-\gamma_3 t}$. Consequently, according to Eq. (2b), the precession frequency exponentially increases in time as:

$$\Omega_2(t) = \frac{\Omega_0^2}{2g(0)} e^{\gamma_3 t}. \quad (3)$$

Note that this description is valid for $g \gg \Omega_0$, and thus we only use Eq. (3) to determine $g(0)$, $\dot{\psi}(0)$ and γ_3 in this parameter regime.

Figure 4(a) shows a ringdown measurement performed at a pressure of 6.3×10^{-5} mbar. The spinning beam is switched back on at $t \approx 12.5$ s (red dashed line), before

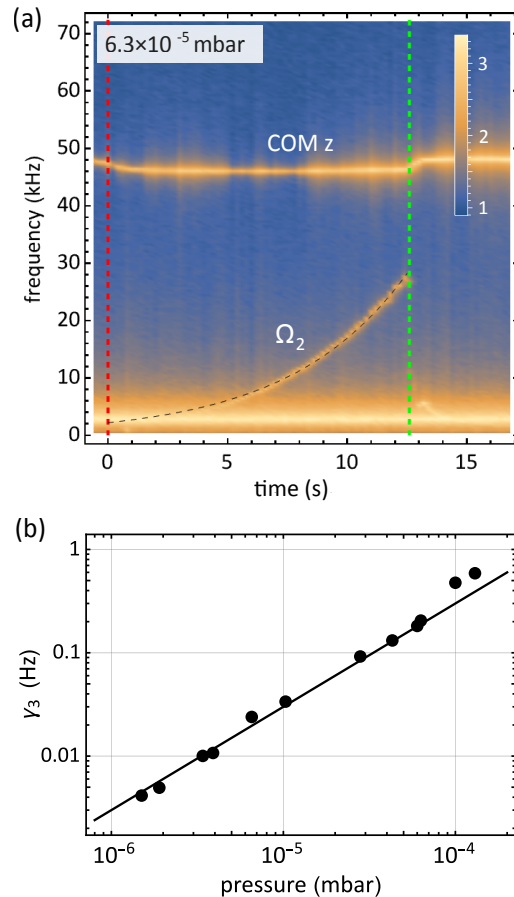


Figure 4. Ringdown measurements for different pressures. (a) PSDs as a function of time t , after blocking the spinning beam (initial power 50 mW) at $t = 0$, marked by the dashed red line. The vacuum pressure is 6.3×10^{-5} mbar. The dumbbell's spinning rate decreases due to friction, which is evidenced by the increase of the precession mode frequency Ω_2 . The time the spinning beam is switched back on is indicated by a dashed green line. Color shows $\log(\text{PSD})$ in arbitrary units. (b): Damping rate γ_3 as a function of pressure extracted from ringdown measurements. Error bars are smaller than the size of the data points. The solid line is a linear fit.

Ω_2 reaches the COM z frequency. The data show that Ω_2 increases exponentially after switching off the spinning beam. From a fit to Eq. (3), shown as a black dashed line, we extract the spinning rate $\dot{\psi}(0) = 2\pi \times 210(7)$ MHz and damping rate $\gamma_3 = 204(2)$ mHz, together with their standard errors.

We repeated similar ringdown measurements for even lower pressures, down to 1.5×10^{-6} mbar, where we reached the exceptionally high spinning rate of $\dot{\psi}(0) = 2\pi \times 1.20(6)$ GHz. The extracted damping rates γ_3 , measured for pressures between 10^{-6} and 10^{-3} mbar, are shown in Fig. 4(b) together with a linear fit [36]. Despite the GHz rotational rates reached, throughout our experiments we did not observe consistent particle

deformations [30].

Conclusion.— We have experimentally achieved controlled spinning of an optically levitated nanodumbbell around its long axis and demonstrated GHz spinning rates and damping rates of a few mHz. This demonstration is of interest for applications in inertial torque sensing. The parameters demonstrated in this work translate into a thermally limited gyroscope sensitivity (angular random walk) of $\Omega_{\text{ARW}} = \sqrt{4k_B T \gamma} / (\sqrt{I_3} \dot{\psi}_0) \approx 4 \times 10^{-6} \text{ rad/s}/\sqrt{\text{Hz}}$ [15], which is only two orders of magnitude larger than the self-noise of the best high-end gyroscopes [37]. Our experiment can be further optimized, e.g. by using larger dumbbells ($\Omega_{\text{ARW}} \propto r^{-5/2}$, where r is the nanoparticle radius) or by lower vacuum pressures.

Our system is fully described by classical dynamics, but we note that recent advances have brought rotational levitodynamics close to the quantum regime [20, 38]. The demonstration of long-axis spinning expands the understanding of the interaction of rotational degrees of freedom with light and provides an important step towards the observation of macroscopic quantum effects [20, 22, 39].

Furthermore, our system can also serve as a platform for studying deep-strong coupling between mechanical modes [40] since the coupling rate g between libration modes, introduced by long-axis spinning, is shown to be nearly three orders of magnitude larger than the natural libration frequency Ω_0 , thereby outperforming the g/Ω_0 values reached with trapped atoms [41].

Acknowledgments.— The authors thank C. Gonzalez-Ballester, J. Harris and members of the Photonics Laboratory for fruitful discussions. This research was supported by the European Union’s Horizon 2020 research and innovation programme under grant agreement No. [863132] (IQLev) and ETH Grant No. ETH-47 20-2. A. Norrman acknowledges support from the Research Council of Finland (Grant Nos. 354918 and 320166). F. van der Laan was supported by the Netherlands Organisation for Scientific Research (NWO).

* www.photonics.ethz.ch

- [1] R. Reimann, M. Doderer, E. Hebestreit, R. Diehl, M. Frimmer, D. Windey, F. Tebbenjohanns, and L. Novotny, GHz rotation of an optically trapped nanoparticle in vacuum, *Phys. Rev. Lett.* **121**, 033602 (2018).
- [2] J. Ahn, Z. Xu, J. Bang, Y.-H. Deng, T. M. Hoang, Q. Han, R.-M. Ma, and T. Li, Optically levitated nanodumbbell torsion balance and ghz nanomechanical rotor, *Phys. Rev. Lett.* **121**, 033603 (2018).
- [3] J. Ahn, Z. Xu, J. Bang, P. Ju, X. Gao, and T. Li, Ultrasensitive torque detection with an optically levitated nanorotor, *Nat. Nanotechnol.* **15**, 89 (2020).
- [4] F. van der Laan, R. Reimann, A. Militaru, F. Tebbenjohanns, D. Windey, M. Frimmer, and L. Novotny, Optically levitated rotor at its thermal limit of frequency stability, *Phys. Rev. A* **102**, 013505 (2020).
- [5] J. Bang, T. Seberson, P. Ju, J. Ahn, Z. Xu, X. Gao, F. Robicheaux, and T. Li, Five-dimensional cooling and nonlinear dynamics of an optically levitated nanodumbbell, *Phys. Rev. Res.* **2**, 043054 (2020).
- [6] F. van der Laan, F. Tebbenjohanns, R. Reimann, J. Vijayan, L. Novotny, and M. Frimmer, Sub-kelvin feedback cooling and heating dynamics of an optically levitated libration, *Phys. Rev. Lett.* **127**, 123605 (2021).
- [7] J. Schäfer, H. Rudolph, K. Hornberger, and B. A. Stickler, Cooling nanorotors by elliptic coherent scattering, *Phys. Rev. Lett.* **126**, 163603 (2021).
- [8] A. Pontin, H. Fu, M. Toroš, T. S. Monteiro, and P. F. Barker, Simultaneous cavity cooling of all six degrees of freedom of a levitated nanoparticle, *Nature Physics* **19**, 1003 (2023).
- [9] Z. Xu and T. Li, Detecting casimir torque with an optically levitated nanorod, *Phys. Rev. A* **96**, 033843 (2017).
- [10] S. Kuhn, B. A. Stickler, A. Kosloff, F. Patolsky, K. Hornberger, M. Arndt, and J. Millen, Optically driven ultra-stable nanomechanical rotor, *Nat. Commun.* **8**, 1670 (2017).
- [11] M. Rashid, M. Toroš, A. Setter, and H. Ulbricht, Precession motion in levitated optomechanics, *Phys. Rev. Lett.* **121**, 253601 (2018).
- [12] P. Ju, Y. Jin, K. Shen, Y. Duan, Z. Xu, X. Gao, X. Ni, and T. Li, Near-field ghz rotation and sensing with an optically levitated nanodumbbell (2023), [arXiv:2301.10868](https://arxiv.org/abs/2301.10868) [quant-ph].
- [13] T. Seberson and F. Robicheaux, Parametric feedback cooling of rigid body nanodumbbells in levitated optomechanics, *Phys. Rev. A* **99**, 013821 (2019).
- [14] K. Zeng, X. Xu, Y. Wu, X. Wu, and D. Xiao, Optically levitated gyroscopes with a mhz rotating micro-rotor (2023), [arXiv:2308.09085](https://arxiv.org/abs/2308.09085) [physics.optics].
- [15] K. Poletkin, Mechanical thermal noise in levitation micro-gyroscopes, in *Levitation Micro-Systems: Applications to Sensors and Actuators* (Springer International Publishing, Cham, 2021) pp. 135–154.
- [16] Y. Arita, M. Mazilu, and K. Dholakia, Laser-induced rotation and cooling of a trapped microgyroscope in vacuum, *Nat Commun* **4**, 2374 (2013).
- [17] Y. Arita, S. H. Simpson, G. D. Bruce, E. M. Wright, P. Zemánek, and K. Dholakia, Cooling the optical-spin driven limit cycle oscillations of a levitated gyroscope, *Commun Phys* **6**, 238 (2023).
- [18] L. Dania, D. S. Bykov, F. Goschin, M. Teller, and T. E. Northup, Ultra-high quality factor of a levitated nanomechanical oscillator (2023), [arXiv:2304.02408](https://arxiv.org/abs/2304.02408) [quant-ph].
- [19] F. Tebbenjohanns, A. Militaru, A. Norrman, F. van der Laan, L. Novotny, and M. Frimmer, Optimal orientation detection of an anisotropic dipolar scatterer, *Phys. Rev. A* **105**, 053504 (2022).
- [20] B. Stickler, K. Hornberger, and M. Kim, Quantum rotations of nanoparticles, *Nat. Rev. Phys.* **3**, 589–597 (2021).
- [21] C. P. Koch, M. Lemesko, and D. Sugny, Quantum control of molecular rotation, *Rev. Mod. Phys.* **91**, 035005 (2019).

- [22] B. A. Stickler, B. Papendell, S. Kuhn, B. Schrinski, J. Millen, M. Arndt, and K. Hornberger, Probing macroscopic quantum superpositions with nanorotors, *New J. Phys.* **20**, 122001 (2018).
- [23] A. Norrman, A. T. Friberg, J. J. Gil, and T. Setälä, Dimensionality of random light fields, *J. Eur. Opt. Soc.-Rapid Publ.* **13**, 36 (2017).
- [24] M. A. Alonso, Geometric descriptions for the polarization of nonparaxial light: a tutorial, *Adv. Opt. Photonics* **15**, 176 (2023).
- [25] K. Y. Bliokh and F. Nori, Transverse and longitudinal angular momenta of light, *Phys. Rep.* **592**, 1 (2015).
- [26] J. J. Gil, A. Norrman, A. T. Friberg, and T. Setälä, Spin of random stationary light, *Phys. Rev. A* **107**, 053518 (2023).
- [27] L. Bellando, M. Kleine, Y. Amarouchene, M. Perrin, and Y. Louyer, Giant diffusion of nanomechanical rotors in a tilted washboard potential, *Phys. Rev. Lett.* **129**, 023602 (2022).
- [28] F. van der Laan, *Rotational Levitodynamics*, Ph.D. thesis, ETH Zurich (2022).
- [29] M. Kamba, R. Shimizu, and K. Aikawa, Nanoscale feedback control of six degrees of freedom of a near-sphere, [arXiv:2303.02831](https://arxiv.org/abs/2303.02831) (2023).
- [30] See Supplemental Material at [URL_will_be_inserted_by_publisher](#) for theoretical considerations, which include Refs. [42-48].
- [31] L. D. Landau and E. M. Lifshitz, *Mechanics, Third Edition: Volume 1 (Course of Theoretical Physics)*, 3rd ed. (Butterworth-Heinemann, 1976).
- [32] A. D. Rider, C. P. Blakemore, A. Kawasaki, N. Priel, S. Roy, and G. Gratta, Electrically driven, optically levitated microscopic rotors, *Phys. Rev. A* **99**, 041802 (2019).
- [33] H. Goldstein, C. Poole, and J. Safko, *Classical Mechanics, 3rd ed.* (Pearson Education, 2001).
- [34] J. Gieseler, B. Deutsch, R. Quidant, and L. Novotny, Subkelvin Parametric Feedback Cooling of a Laser-Trapped Nanoparticle, *Physical Review Letters* **109**, 103603 (2012).
- [35] J. A. Zielińska, F. van der Laan, A. Norrman, M. Rimplinger, R. Reimann, L. Novotny, and M. Frimmer, Controlling optomechanical libration with the degree of polarization, *Phys. Rev. Lett.* **130**, 203603 (2023).
- [36] L. Martinetz, K. Hornberger, and B. A. Stickler, Gas-induced friction and diffusion of rigid rotors, *Phys. Rev. E* **97**, 052112 (2018).
- [37] iXblue, [blueSeis-3A Portable rotational 3-component seismometer, absolute and broadband](#) (2022).
- [38] C. Gonzalez-Ballester, M. Aspelmeyer, L. Novotny, R. Quidant, and O. Romero-Isart, Levitodynamics: Levitation and control of microscopic objects in vacuum, *Science* **374**, eabg3027 (2021).
- [39] Y. Ma, K. E. Khosla, B. A. Stickler, and M. S. Kim, Quantum persistent tennis racket dynamics of nanorotors, *Phys. Rev. Lett.* **125**, 053604 (2020).
- [40] A. Frisk Kockum, A. Miranowicz, S. De Liberato, S. Savasta, and F. Nori, Ultrastrong coupling between light and matter, *Nature Reviews Physics* **1**, 19 (2019), 1807.11636.
- [41] J. Koch, G. R. Hunanyan, T. Ockenfels, E. Rico, E. Solano, and M. Weitz, Quantum Rabi dynamics of trapped atoms far in the deep strong coupling regime, *Nature Communications* **14**, 954 (2023).
- [42] E. W. Weisstein, Euler angles, [From MathWorld—A Wolfram Web Resource](#) .
- [43] L. Novotny and B. Hecht, *Principles of Nano-Optics*, 2nd ed. (Cambridge University Press, 2012).
- [44] I. Toftul, G. Fedorovich, D. Kislov, K. Frizyuk, K. Koshelev, Y. Kivshar, and M. Petrov, Nonlinearity-induced optical torque, *Phys. Rev. Lett.* **130**, 243802 (2023).
- [45] R. Kitamura, L. Pilon, and M. Jonasz, Optical constants of silica glass from extreme ultraviolet to far infrared at near room temperature, *Appl. Opt.* **46**, 8118 (2007).
- [46] F. Monteiro, S. Ghosh, E. C. van Assendelft, and D. C. Moore, Optical rotation of levitated spheres in high vacuum, *Phys. Rev. A* **97**, 051802 (2018).
- [47] M. Schuck, D. Steinert, T. Nussbaumer, and J. W. Kolar, Ultrafast rotation of magnetically levitated macroscopic steel spheres, *Science Advances* **4**, e1701519 (2018), <https://www.science.org/doi/pdf/10.1126/sciadv.1701519>.
- [48] D. Hümmer, R. Lampert, K. Kustura, P. Maurer, C. Gonzalez-Ballester, and O. Romero-Isart, Acoustic and optical properties of a fast-spinning dielectric nanoparticle, *Phys. Rev. B* **101**, 205416 (2020).

Supporting Information: Long-axis spinning of an optically levitated particle: A levitated spinning top

J. A. Zielińska,¹ F. van der Laan,^{1,2} A. Norrman,^{1,3} R. Reimann,^{1,4} M. Frimmer,¹ and L. Novotny^{1,*}

¹*Photonics Laboratory, ETH Zürich, CH-8093 Zürich, Switzerland*

²*Center for Nanophotonics, AMOLF, 1098 XG Amsterdam, The Netherlands*

³*Center for Photonics Sciences, University of Eastern Finland, P.O. Box 111, FI-80101 Joensuu, Finland*

⁴*Quantum Research Center, Technology Innovation Institute, Abu Dhabi, UAE*

(Dated: March 18, 2024)

I. PARTICLE DESCRIPTION

In this work we focus on nanodumbbell particles, which are cylindrically symmetric objects comprised of two spheres attached to each other. We assume that the moment of inertia tensor as well as the real and imaginary parts of the polarizability tensor can be simultaneously diagonalized in the principal axes reference frame of the particle. We refer to this frame of reference as the "particle frame" and represent the principal axes by the unit vectors $(\mathbf{e}_1, \mathbf{e}_2, \mathbf{e}_3)$. We further let $\boldsymbol{\alpha}' = \text{diag}(\alpha'_1, \alpha'_1, \alpha'_3)$ and $\boldsymbol{\alpha}'' = \text{diag}(\alpha''_1, \alpha''_1, \alpha''_3)$ denote the real and imaginary parts of the static polarizability tensor of the object in the intrinsic body frame, respectively, assuming $\alpha'_1 < \alpha'_3$. The moment of inertia of the particle is described by the tensor $\mathbf{I} = \text{diag}(I_1, I_1, I_3)$, where we assume $I_1 > I_3$. We refer to \mathbf{e}_3 (the principal axis with the largest polarizability) as the "long axis" of the object.

In order to describe the orientation of the particle frame with respect to the laboratory frame (x, y, z) , we use the intrinsic x -convention of Euler angles denoted as ϕ , θ and ψ (see [1] and §35 in [2]). The Euler angles ϕ and θ describe the orientation of the long axis of the rotor. In turn, the Euler angle ψ describes rotation of the nanodumbbell around its long axis, i.e., ψ is the spinning speed. The angle measured in the experiment is ϕ , which corresponds to the orientation of the long axis in the xy plane with respect to the y axis.

In order to transform a vector from the laboratory to the particle frame we first rotate it by the angle ϕ around z , then by θ around \mathbf{e}_1 and finally by ψ around \mathbf{e}_3 . The transformation matrix \mathbf{R} corresponding to these three rotation operations is given in [1].

II. CONSERVATIVE TORQUES

In this section we calculate the potential arising from the real part $\boldsymbol{\alpha}'$ of the polarizability tensor of the particle. The libration dynamics is dictated by the direction of the electric dipole moment induced by the optical field, whose orientation depends on the particle orientation and in general is not parallel to the electric field.

We describe the electric field of the linearly polarized trapping beam at the tweezers focal point as $\mathbf{E}_t = (E_t e^{i\omega_t t}, 0, 0)^T$. In turn, we can write the electric field of the spinning beam (also at the tweezers focal point) as $\mathbf{E}_s = (0, E_s e^{i\omega_s t}, iE_s e^{i\omega_s t})^T$. The dipole moment induced on the trapped anisotropic particle, expressed in the laboratory frame, is given by

$$\mathbf{p} = \mathbf{R}^{-1} \boldsymbol{\alpha}' \mathbf{R} \mathbf{E}, \quad (\text{S1})$$

where $\mathbf{E} = \mathbf{E}_t + \mathbf{E}_s$ is also expressed in the laboratory reference frame. Since in general \mathbf{p} and \mathbf{E} are not parallel, the potential energy U associated with the orientation of the particle (after averaging over optical frequencies) is

$$U = -\frac{1}{4} \text{Re}(\mathbf{p} \cdot \mathbf{E}^*). \quad (\text{S2})$$

Due to the fact that the trapping and spinning fields oscillate at different optical frequencies ω_t and ω_s , corresponding to their respective wavelengths $\lambda_t = 1550$ nm and $\lambda_s = 1064$ nm, we can average out the cross terms oscillating at $\omega_s - \omega_t$ and calculate the potential components arising from both components independently. The potential arising from the trapping beam then reads

$$U_t = -\frac{1}{4} E_t^2 (\alpha'_1 + \Delta\alpha' \sin^2 \phi \sin^2 \theta), \quad (\text{S3})$$

* www.photonics.ethz.ch

where $\Delta\alpha' = \alpha'_3 - \alpha'_1$. The term U_t aligns the long axis of the particle with the trapping beam electric field, which points along x axis. The potential arising from the spinning beam is

$$U_s = -\frac{1}{4}E_s^2 (\alpha'_1 + \alpha'_3 - \Delta\alpha' \sin\phi^2 \sin\theta^2). \quad (\text{S4})$$

In turn, the potential term U_s tries to align the long axis of the particle to the yz plane, thus counteracting U_t . However, since the trapping field is much stronger than the spinning beam, $|E_t|^2 \gg |E_s|^2$, we can approximate the total potential as $U \approx U_t$.

The long axis of the dumbbell oscillates in the potential minimum, occurring for $\phi = \theta = \pi/2$, which gives rise to two libration modes $\vartheta = \theta - \pi/2$ and $\varphi = \phi - \pi/2$. Expanding the potential around minimum and removing orientation-independent terms leads to

$$U \approx \frac{1}{2}I_1\Omega_0^2 (\varphi^2 + \vartheta^2), \quad (\text{S5})$$

where $\Omega_0 = \sqrt{\Delta\alpha E_t^2/2I_1}$ denotes the libration frequency.

Finally, let us describe the libration dynamics due to the potential U in terms of the restoring torque κ , whose components in the particle frame read

$$\kappa_1 = -I_1\Omega_0^2(\vartheta \cos\psi + \varphi \sin\psi), \quad (\text{S6a})$$

$$\kappa_2 = -I_1\Omega_0^2(-\vartheta \sin\psi + \varphi \cos\psi), \quad (\text{S6b})$$

$$\kappa_3 = 0. \quad (\text{S6c})$$

Note that the restoring torque components in the particle frame of reference depend on angle ψ , describing the rotation of the particle around its long axis.

III. NON-CONSERVATIVE TORQUE

The non-conservative dynamics in our experiment arises from the circular polarization of the spinning beam, which provides constant torque spinning the particle around its long axis. This torque can arise from optical absorption or scattering [3] and depends on the x component of the optical spin $S_x = \text{Im} \langle \mathbf{E}^* \times \mathbf{E} \rangle_x$ of the focused electric field \mathbf{E} at the location of the dumbbell. The torque from absorption relies on the imaginary part of the dumbbell polarizability and is given by $\tau_{\text{abs}} = \frac{1}{2}\alpha''_3 S_x$.

Optical torque transfer by scattering requires some optical anisotropy that breaks the dumbbell's cylindrical symmetry. The scattering torque is given by $\tau_{\text{sc}} = \frac{1}{2}(\delta\alpha')^2 g_{\text{sc}} S_x$ [3], where $\delta\alpha'$ is a measure for the optical anisotropy and $g_{\text{sc}} = \omega^3/(6\pi\epsilon_0 c^3)$. This anisotropy could arise from a deviation from the perfectly spherical shape of the two particles constituting the dumbbell [4].

Regardless of the mechanism of the angular momentum transfer from the light to the particle, we describe the effect of the circularly polarized spinning beam propagating along x as a constant torque $\boldsymbol{\tau} = (\tau, 0, 0)$ in the lab frame. We expect the torque magnitude to be proportional to the spinning beam power, in other words $\tau \propto |E_s|^2$. The components of $\boldsymbol{\tau}$ in the particle frame read:

$$\tau_1 = (-\varphi \cos\psi + \vartheta \sin\psi)\tau, \quad (\text{S7a})$$

$$\tau_2 = (\vartheta \cos\psi + \varphi \sin\psi)\tau, \quad (\text{S7b})$$

$$\tau_3 = \tau, \quad (\text{S7c})$$

where we have expanded to the first order around the particle orientation in the potential minimum (set by the trapping beam).

Therefore, the total torque \mathbf{K} experience by our particle, which includes both the conservative torque arising from the potential U and non-conservative spinning torque $\boldsymbol{\tau}$ amounts to

$$K_1 = \tau_1 + \kappa_1 \approx -I_1\Omega_0^2(\vartheta \cos\psi + \varphi \sin\psi), \quad (\text{S8a})$$

$$K_2 = \tau_2 + \kappa_2 \approx -I_1\Omega_0^2(-\vartheta \sin\psi + \varphi \cos\psi), \quad (\text{S8b})$$

$$K_3 = \tau_3 + \kappa_3 \approx \tau. \quad (\text{S8c})$$

when expressed in the particle frame of reference. We have neglected the terms τ_1 and τ_2 [see Eqs. (S7a) and (S7b)], which introduce a small coupling between libration modes φ and ϑ . This coupling has a negligible effect on the libration dynamics (dominated by the strong coupling introduced by the spinning motion), as $|E_s|^2 \ll |E_t|^2$ implies that $\tau \ll I_1\Omega_0^2$.

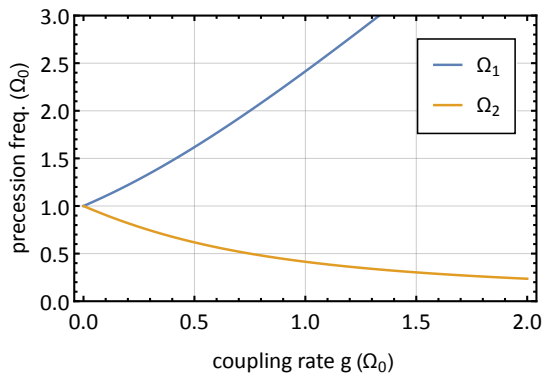


FIG. S1. Precession modes Ω_1 and Ω_2 calculated from Eq. (S14) in the units of natural libration frequency Ω_0 .

IV. EQUATIONS OF MOTION

This section contains the analysis of the Euler equations of motion in presence of the torque derived in the previous section. We begin by expressing the angular velocity ω in the particle frame and expanding it to the first order in libration angles φ and ϑ :

$$\omega_1 \approx \dot{\varphi} \sin \psi + \dot{\vartheta} \cos \psi, \quad (\text{S9a})$$

$$\omega_2 \approx \dot{\varphi} \cos \psi - \dot{\vartheta} \sin \psi, \quad (\text{S9b})$$

$$\omega_3 \approx -\dot{\varphi}\vartheta + \dot{\psi}. \quad (\text{S9c})$$

In the remainder of this work we are interested in the regime of large $\dot{\psi}$ and small-amplitude libration, therefore we further approximate the third component of the angular velocity as $\omega_3 \approx \dot{\psi}$.

Particle-frame Euler equations of motion for our cylindrically symmetrical dumbbell read:

$$K_1 = I_1 \dot{\omega}_1 - \Delta I \omega_2 \omega_3, \quad (\text{S10a})$$

$$K_2 = I_1 \dot{\omega}_2 + \Delta I \omega_1 \omega_3, \quad (\text{S10b})$$

$$K_3 = I_3 \dot{\omega}_3, \quad (\text{S10c})$$

where $\Delta I = I_1 - I_3$. Using the expressions for torque (see Eqs. (S8a)–(S8c)) and angular velocity (see Eqs. (S9a)–(S9c)) components, we can rewrite Eqs. (S10a)–(S10c) as:

$$I_1 \ddot{\vartheta} + I_3 \dot{\varphi} \dot{\psi} = -I_1 \Omega_0^2 \vartheta, \quad (\text{S11a})$$

$$I_1 \ddot{\varphi} - I_3 \dot{\vartheta} \dot{\psi} = -I_1 \Omega_0^2 \varphi, \quad (\text{S11b})$$

$$I_3 \ddot{\psi} = \tau. \quad (\text{S11c})$$

Note that Eqs. (S11a) and (S11b) describe two coupled harmonic oscillators ϑ and φ , whereas according the Eq. (S11c), the velocity of the spinning around the long axis $\dot{\psi}$ increases to infinity. In order to avoid this problem, we have to expand the model to include friction in Eq. (S11c). In presence of friction (described by coefficient γ_3), the spinning speed $\dot{\psi}$ will increase until it reaches a stationary value $\dot{\psi}_0 = \tau / (I_3 \gamma_3)$, for which driving torque τ is balanced by the friction [5, 6].

V. COUPLED LIBRATION MODES

Let us now focus on the coupled libration modes described by Eqs. (S11a) and (S11b) and rewrite them explicitly introducing the coupling rate g ,

$$\ddot{\vartheta} + 2g\dot{\varphi} = -\Omega_0^2 \vartheta, \quad (\text{S12a})$$

$$\ddot{\varphi} - 2g\dot{\vartheta} = -\Omega_0^2 \varphi, \quad (\text{S12b})$$

where $g = (I_3/2I_1)\dot{\psi}_0$. In agreement with [7], the solution can be written as

$$\vartheta = \alpha_1 \cos(\Omega_1 t + \delta_1) + \alpha_2 \cos(\Omega_2 t + \delta_2), \quad (\text{S13a})$$

$$\varphi = \alpha_1 \sin(\Omega_1 t + \delta_1) - \alpha_2 \sin(\Omega_2 t + \delta_2) \quad (\text{S13b})$$

where $\alpha_{1/2}$ and $\delta_{1/2}$ depend on initial angular displacements and velocities and the eigenfrequencies read

$$\Omega_{1/2} = \sqrt{\Omega_0^2 + g^2} \pm g. \quad (\text{S14})$$

Note that the fast precession (nutation) mode with frequency Ω_1 corresponds to a circular motion of the long axis in the counterclockwise direction (for τ pointing along the positive x direction), and the slow precession mode corresponds to a clockwise long axis motion.

The dependence of $\Omega_{1/2}$ on the coupling rate g is shown in Fig. S1. For a fast spinning dumbbell ($g \gg \Omega_0$) the frequencies can be approximated as:

$$\Omega_1 = 2g, \quad (\text{S15a})$$

$$\Omega_2 = \frac{\Omega_0^2}{2g}. \quad (\text{S15b})$$

Finally, let us turn our attention to the amplitudes of precession and nutation. For a rapidly spinning top, the ratio between the amplitude of nutation α_1 and the amplitude of precession α_2 decreases proportionally to the spinning speed $\dot{\psi}$ squared [8]. Therefore we expect nutation will be negligible for a rapidly spinning dumbbell and the dynamics will be dominated by slow precession with frequency Ω_2 . The amplitude of the slow precession α_2 is equivalent to the tilt between the long axis of the dumbbell and x axis. This angle will stay almost constant as the dumbbell precesses, except for fast, small-amplitude oscillations caused by nutation. The effective potential governing the motion of the tilt angle α_2 can be written as $U_{\text{ef}} = \frac{1}{2}I_1(g^2 + \Omega_0^2)\alpha_2^2$ [2]. Applying equipartition theorem to this degree of freedom allows us to predict the average precession amplitude (tilt angle) of the thermally driven spinning top, which yields:

$$\langle \alpha_2^2 \rangle = \frac{k_B T}{I_1(\Omega_0^2 + g^2)} \quad (\text{S16})$$

Comparing the above result with Eq. S13b indicates that the oscillation amplitude of the libration angle φ measured in our experiment will behave similarly (if the angular degrees of freedom except ψ are in thermal equilibrium with the surrounding gas). To summarize, we expect that both the amplitude of the nutation and precession will diminish as we increase the spinning speed, with nutation signal diminishing much faster. In practice, the amplitude of precession motion may be affected by misalignment between the spinning beam and the tweezers' polarization and external rotation of the experimental apparatus (e.g. due to the floating optical table).

VI. THE SPINNING TORQUE

We estimate that the magnitude of the spin vector $\text{Im} \langle \mathbf{E}_s^* \times \mathbf{E}_s \rangle$ [9] carried by the spinning beam can reach up to $5 \times 10^{12} \text{ V}^2/\text{m}^2$. For comparison, the electric field squared corresponding to the trapping beam at the focal spot is 200 times larger. Additionally, it is interesting to compare the spin angular momentum carried by the spinning field to the transverse spin generated by focusing the linearly polarized trapping beam near the trapping region [10, 11]—in our experiment the angular momentum of the spinning beam is an order of magnitude smaller.

The damping rates γ_3 and the spinning rates extracted from the ringdown measurements (see main text) allow us to estimate the torque exerted on the dumbbell by a circularly polarized beam, arriving at $\tau = 5 \times 10^{-25} \text{ N m}$ for 100 mW of the optical power. The torque value remained consistent across different dumbbells used in our experiments. We are unable to determine whether the torque arises from optical absorption, scattering (which requires breaking the cylindrical symmetry of the dumbbell) or other processes [12]. Attributing this torque to absorption requires the dumbbell's absorption coefficient to be two orders of magnitude larger than expected for bulk silica at 1064 nm [13]. On the other hand, attributing the torque to the scattering process [3], requires the polarizability of the dumbbell along the two short axes to differ by approximately 3%. Both increased absorption and imperfect spherical shape of the silica nanoparticles have been reported by other researchers [4, 14].

VII. PARTICLE DEFORMATION DUE TO CENTRIFUGAL FORCES

The calculated tensile stress generated by centrifugal force in silica nanodumbbells in our experiments reaches 0.5 GPa [5, 15], and approaches the regime of deforming the particle shape [16]. However, no consistent changes in characteristic frequencies and damping rates, temporary or permanent, were observed. We have recorded a single case of deformation (out of ~ 15 dumbbells investigated in total). After spinning with approx. 200 MHz, the particle's x -to- y gas damping ratio changed from 1.14 to 1.07, and the natural libration frequency decreased by 35%. The data obtained from this particle is not used in the manuscript.

-
- [1] E. W. Weisstein, Euler angles, [From MathWorld—A Wolfram Web Resource](#) .
 - [2] L. D. Landau and E. M. Lifshitz, *Mechanics, Third Edition: Volume 1 (Course of Theoretical Physics)*, 3rd ed. (Butterworth-Heinemann, 1976).
 - [3] L. Bellando, M. Kleine, Y. Amarouchene, M. Perrin, and Y. Louyer, Giant diffusion of nanomechanical rotors in a tilted washboard potential, *Phys. Rev. Lett.* **129**, 023602 (2022).
 - [4] M. Kamba, R. Shimizu, and K. Aikawa, Nanoscale feedback control of six degrees of freedom of a near-sphere, [arXiv:2303.02831 \(2023\)](#).
 - [5] R. Reimann, M. Doderer, E. Hebestreit, R. Diehl, M. Frimmer, D. Windey, F. Tebbenjohanns, and L. Novotny, Ghz rotation of an optically trapped nanoparticle in vacuum, *Phys. Rev. Lett.* **121**, 033602 (2018).
 - [6] J. Ahn, Z. Xu, J. Bang, Y.-H. Deng, T. M. Hoang, Q. Han, R.-M. Ma, and T. Li, Optically levitated nanodumbbell torsion balance and ghz nanomechanical rotor, *Phys. Rev. Lett.* **121**, 033603 (2018).
 - [7] T. Seberson and F. Robicheaux, Parametric feedback cooling of rigid body nanodumbbells in levitated optomechanics, *Phys. Rev. A* **99**, 013821 (2019).
 - [8] H. Goldstein, C. Poole, and J. Safko, *Classical Mechanics, 3rd ed.* (Pearson Education, 2001).
 - [9] J. J. Gil, A. Norrman, A. T. Friberg, and T. Setälä, Spin of random stationary light, *Phys. Rev. A* **107**, 053518 (2023).
 - [10] L. Novotny and B. Hecht, *Principles of Nano-Optics*, 2nd ed. (Cambridge University Press, 2012).
 - [11] J. A. Zielińska, F. van der Laan, A. Norrman, M. Rimplinger, R. Reimann, L. Novotny, and M. Frimmer, Controlling optomechanical libration with the degree of polarization, *Phys. Rev. Lett.* **130**, 203603 (2023).
 - [12] I. Toftul, G. Fedorovich, D. Kislov, K. Frizyuk, K. Koshelev, Y. Kivshar, and M. Petrov, Nonlinearity-induced optical torque, *Phys. Rev. Lett.* **130**, 243802 (2023).
 - [13] R. Kitamura, L. Pilon, and M. Jonasz, Optical constants of silica glass from extreme ultraviolet to far infrared at near room temperature, *Appl. Opt.* **46**, 8118 (2007).
 - [14] F. Monteiro, S. Ghosh, E. C. van Assendelft, and D. C. Moore, Optical rotation of levitated spheres in high vacuum, *Phys. Rev. A* **97**, 051802 (2018).
 - [15] M. Schuck, D. Steinert, T. Nussbaumer, and J. W. Kolar, Ultrafast rotation of magnetically levitated macroscopic steel spheres, *Science Advances* **4**, e1701519 (2018), <https://www.science.org/doi/pdf/10.1126/sciadv.1701519>.
 - [16] D. Hümmer, R. Lampert, K. Kustura, P. Maurer, C. Gonzalez-Ballester, and O. Romero-Isart, Acoustic and optical properties of a fast-spinning dielectric nanoparticle, *Phys. Rev. B* **101**, 205416 (2020).